# Application of Fourier Transform Profilometry in Pulmonary Function Testing

M. Leonardi, M. Fležar*, A. Urbanč, J. Lenarčič

Jožef Stefan Institute, Ljubljana, Slovenija
* UKC, Ljubljana, Slovenija

This paper compares Fourier Transform Profilometry, a computer based technique for automatic 3–D measurement, with conventional Moiŕe techniques. In Moiré contouring techniques two gratings are used to generate Moiré fringes. In contrast to that in FTP a grating pattern projected onto the object surface is Fourier transformed and processed. Results are analysed and some alternative tests are presented. In addition to that an application in medicine is proposed for pulmonary function testing. Several measurements of lung relaxation pressure by observing the depression of skin between ribs have been performed.

## 1. Introduction

The goal of our work was to select a 3–D measuring method based on use of computer vision that can be used for measuring anthropometric properties of human body. In selecting the appropriate method, the following criteria was used: suitability of the method to measure 3–D shape of the human body, system's accuracy, price of needed measuring equipment, fleksibility, and reliability of the system. For use in anthropometry are active range measuring methods more appropriate than passive. The advantages of active methods are: insensitivity to the changes in brightness of the scene, greater accuracy of the depth perception, easier implementation of the measuring techniques. The fact that passive methods don't use human visual system can be of advantage, since it helps us to detect some parameters invisible to the human eye. Moiré Topography became known after papers of Meadows, Johnson, and Allen [1] and Takasaki [2] is perhaps the simplest way to obtain 3–D information. Since '70s it has been widely used in detection of scoliosis and other deformities of the human back. Methods based on Moiré Topography are also a topic of a symposium on surface topography (Surface Topography and Body Deformity [7]). Fourier Transform Profilometry (FTP) [4, 5] drew attention in the 80's, because of its easy use in atomated processing along with other advantages over standard Moiré techniques. We tested this technique, compared it to Moiré Topography, and used it in pulmonary function testing. Last part of the paper offers mechanics of the human breathing, which is necessary to understand problems in pulmonary function testing. Some experiments are also presented.

## 2. Moiré Topography

Moiré Topography [2] is based on Moiré effect. Moiré patterns occur when two periodical gratings lie on top of the other. The Moiré effect can be seen practically every day on television, whenever an unexpirienced announcer or an ill advised politician appears wearing a stripped jacket. Constantly alternating, oblique lines seem to cover his clothing.

### 2.1. Shadow Moiré

Figure 1 shows a schematic diagram of shadow Moiré setup. An equispaced plane grating is placed in front of the object. The object is illuminated by a point light source (point $S$) and observed from point $O$. If the illumination point

and the observation point are at the same finite distance from the grid ($l$ in the figure), then the fringes which appear on the object are formed by the points of equal distance (contours). The level of contours should be indexed in order to obtain the depth of the image.

The depth of a point positioned at a distance $h_n$ is given by

$$h_n = \frac{nlp}{d - np}, \qquad (1)$$

where $n$ is the level (index) of the current contour, $d$ is the distance between the illumination point and the observation point, $l$ is the distance between the observation (or illumination) point and the grating, and $p$ is the pitch of the grating.

## 2.2. Projection Moiré

Shadow Moiré proved to be working in measuring shapes of relatively small objects. As an alternative method named Projection Moiré [3] was developed. In figure 2 shows schematic setup for a projection Moiré.

In projection Moiré a grating is projected on the object and observed through another grating placed in front of the camera lens. For automatic use by computer this second grating can

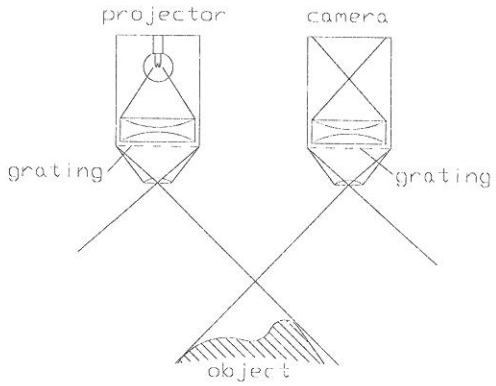


*Fig. 2.* Schematic setup for Projection Moiré

also be simulated. The procedure to obtain the height distribution is quite complicated and includes space transformations. Since it is not important for our consideration, it will not be explained here. The detailed description of the procedure is given in [3].

## 3. Fourier Transform Profilometry

### 3.1. Optical Geometry

In our experiments, the so called crossed-optical-axes geometry is used. Here the optical axes of

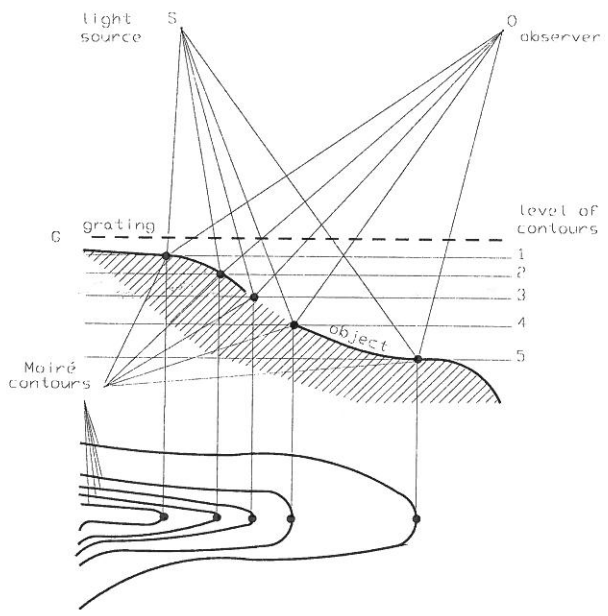


*Fig. 1.* Generation of contours at Shadow Moiré

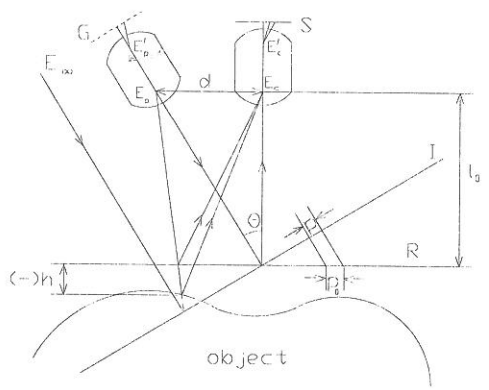


*Fig. 3.* Crossed optical axes geometry

a projector and a camera lie in the same plane and intersect a point near a center of the object.

Figure 3 shows a geometry used in our experiments. When the object is a flat and uniform plane on $R$, $(h = 0)$, and if $E_p$ is at infinity, the grating image projected on an image surface and observed through point $E$ is a regular grating pattern and can be expressed by a Fourier series expansion:

$$g_T(x,y) = \sum_{n=-\infty}^{\infty} A_n \exp(2\pi i n f_0 x) \quad (2)$$

where

$$f_0 = 1/p_0 = cos\theta/p \quad (3)$$

is the fundamental frequency of the observed grating image. If $E_p$ is at finite distance is the pitch increased with $x$ at the image sensor plane. In that case the deformed grating image for $h(x,y) = 0$ can be expressed as

$$g_0(x,y) = \sum_{n=-\infty}^{\infty} A_n \exp\{2\pi i n f_0[x+s_0(x)]\} \quad (4)$$

where $s_0(x) = \overline{BC}$ is a function of $x$ and has a positive sign when $C$ is right to $B$ as in the figure. For simplification we can express Eq.(4) as

$$g_0(x,y) = \sum_{n=-\infty}^{\infty} A_n \exp\{2\pi i n f_0[x+s_0(x)]\} \quad (5)$$

For a general object with varying $h(x,y)$ the deformed grating image is given by

$$g(x,y) = r(x,y) \sum_{n=-\infty}^{\infty} A_n \exp\{i[2\pi n f_0 x + n\phi(x,y)]\} \quad (6)$$

### 3.2. Fourier Transform Method

The deformed grating image given by Eq.(6) can be interpreted as multiple signals with spatial carrier frequencies $nf_0$ modulated both in phase $(\phi_0)$ and amplitude $(r(x,y))$. Since the phase carries information about the 3–D shape to be measured, the problem is how to separate phase $(\phi_0)$ from the unwanted amplitude variation $(r(x,y))$ caused by nonuniform reflectivity of the object surface. We rewrite Eq.(6) as

$$g(x,y) = \sum_{n=-\infty}^{\infty} q_n(x,y) \exp(2\pi i n f_0 x) \quad (7)$$

where

$$q_n(x,y) = A_n r(x,y) \exp[in\phi(x,y)] \quad (8)$$

With use of the FFT, 1–D Fourier transform of Eq.(8) is computed for variable $x$ only, with $y$ being fixed:

$$\begin{aligned} G(f,y) &= \int_{-\infty}^{\infty} g(x,y) \exp(-2\pi i f x) dx \\ &= \int_{-\infty}^{\infty} Q_n(f - nf_0, y) \end{aligned} \quad (9)$$

Here $G(f,y)$ and $Q_n(f,y)$ are 1–D Fourier spectra of $g(x,y)$ and $q_n(x,y)$. Normally all the spectra $Q_n(f - nf_0, y)$ are separated from each other by the carrier frequency (figure 4). Only one spectrum is selected $(Q_1(f - f_0, y))$ and its inverse Fourier transform is computed.

$$\begin{aligned} \hat{g}(x,y) &= q_1(x,y) \exp(2\pi i f_0 x) \\ &= A_1 \exp\{i[2\pi f_0 x + \phi(x,y)]\} \end{aligned} \quad (10)$$

and from Eq.(5)

$$\hat{g}(x,y) = A_1 \exp\{i[2\pi f_0 x + \phi_0(x)]\} \quad (11)$$

and finally

$$\begin{aligned} \hat{g}(x,y)\hat{g}_0^*(x,y) &= |A_1|^2 r(x,y) \\ &\quad \exp\{i[\Delta\phi(x,y)]\} \end{aligned} \quad (12)$$

where

$$\Delta\phi(x,y) = \phi(x,y) - \phi_0(x, y = 0) \quad (13)$$

Since the initial phase distribution $\phi_0(x, y = 0)$ is now subtracted, $\Delta\phi(x,y)$ gives the phase modulation which responds to the object height distribution. Therefore, it should be obtained from the equation (12). This is done by

$$\begin{aligned} &\log[\hat{g}(x,y)\hat{g}_0^*(x,y)] \\ &= \log[|A_1|^2 f(x,y)] + i\Delta\phi(x,y) \end{aligned} \quad (14)$$

### 3.3. Phase-to-Height Conversion

Since phase calculation by computer gives principal values ranging from $-\pi$ to $\pi$, the phase

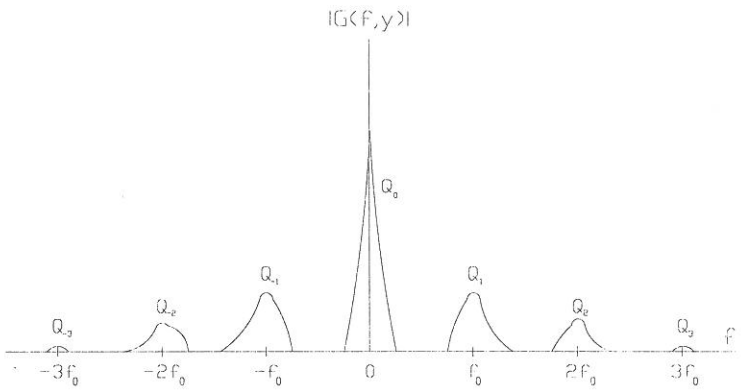


*Figure 4:* Spatial frequency spectra of deformed grating image

distribution is wrapped and has discontinuities with $2\pi$ phase jumps for variations more than $2\pi$. These discontinuties can be corrected by adding or subtracting $2\pi$ according to the phase jump (figure 5). 2–D phase distribution can be obtained simply by repeating the same procedure for $y$ sections.

The phase-to-height conversion formula is

$$h(x,y) = \frac{l_0 p_0[\Delta\phi(x,y)/2\pi]}{p_0[\Delta\phi(x,y)/2\pi] - d} \qquad (15)$$

Maximum range measurable by FTP is limited by the fact that the carrier frequency must separate this spectrum from all other spectra. The condition for the maximum range of measurement is given by

$$\left|\frac{\partial h(x,y)}{\partial x}\right|_{max} < \frac{1}{3}\frac{l_0}{d} \qquad (16)$$

This condition states, that the maximum range of measurement is not limited by the height distribution $h(x,y)$ itself but by its derivative in the direction normal to the line of the grating.

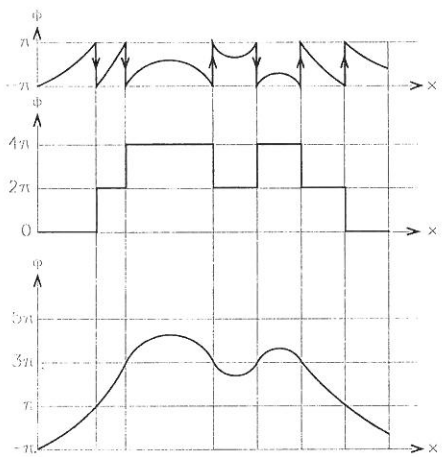


*Fig. 5.* 1–D phase unwrapping

### 3.4. Moiré Topography vs. Fourier Transform Profilometry

Although Fourier Transform Profilometry is often considered to be just one of the techniques, which use Moiré fringes to determine object shape, it has many advantages over ordinary Moiré Topography. These are:

- it makes automatic distinction between a depression and elevation from a contour map of the object,
- no need to assign the fringe orders, there is need to do phase unwrapping instead,
- no need to locate the center lines of broad fringes, since it calculates depth for every point on the image,

- for the same reason, there is no need to interpolate the regions between the contour lines
- it has a much higher sensitivity than ordinary Moiré techniques,
- it can detect height variations less than the amount of one fringe difference
- it is free from effect of the reflectivity of the measured object,
- it is much more appropriate for automated data processing.

Differences between the results obtained by both methods can be seen on figure 6.

### 3.5. Experiments

Figure 7 shows a schematic diagram of the experimental setup. Grating image was projected with a standard slide projector, using slides with a frequency (35 lin/cm). The distance between the camera and the object was 130 cm, camera — projector 30 cm.

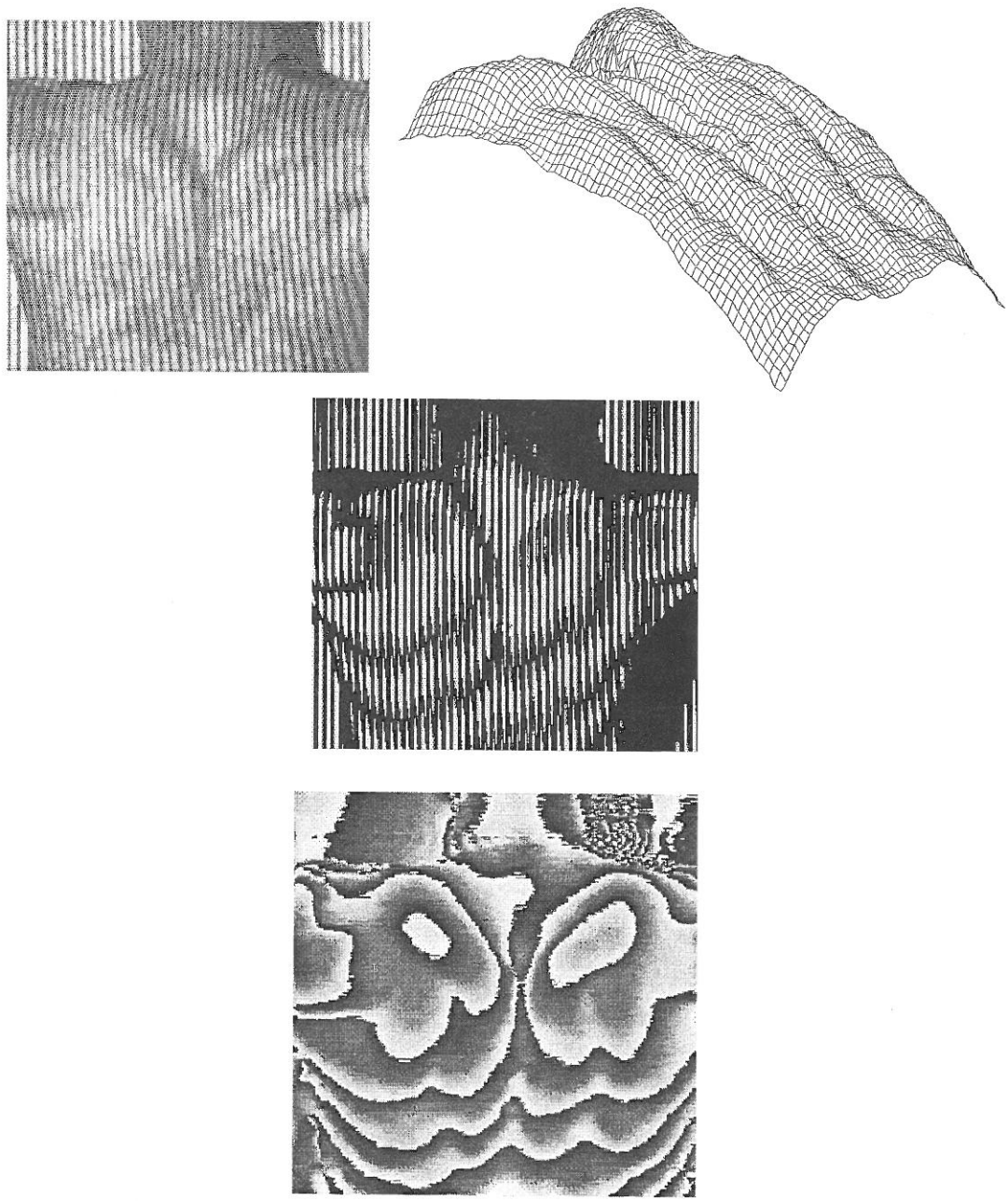

*Fig. 6.* Middle: Moiré contour lines on human back; down: contour lines obtained by same equipment with the use of FTP; up: a deformed grating image and a 3–D presentation of human back

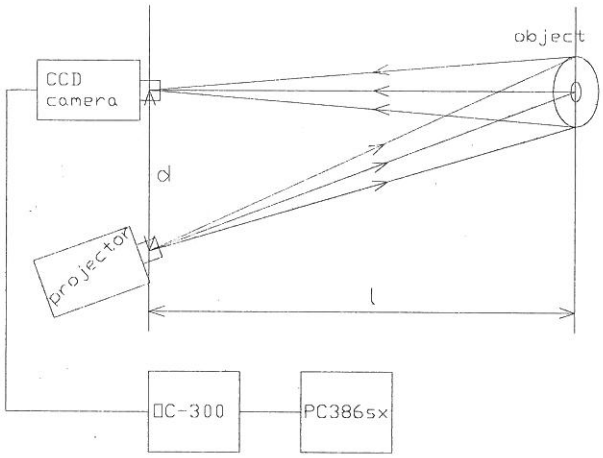


*Fig. 7.* Schematic diagram of the experimental setup

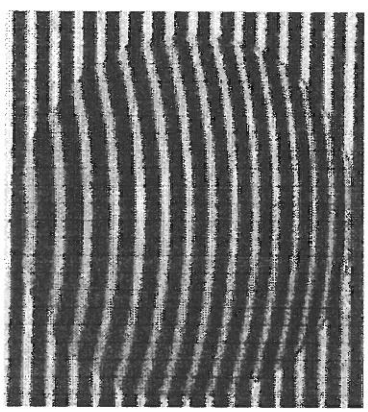

*Fig. 8.* Image of the measured object with projected lines

Figure 8 shows measured object with the projected lines. Wrapped phase distribution is presented in figure 9. Figure 10 shows unwrapped phase distribution. Comparison of results obtained by FTP with those obtained by contact measurement is shown in figure 11.

## 4. Pulmonary Function Testing

### 4.1. Mechanics of Breathing

To move air into the lungs, the respiratory muscles must develop sufficient force to overcome the impedances of the respiratory apparatus (the lungs, the chest cage, and the abdominal contents). Figure 12 shows mechanical analogue of the resistances that must be overcome during breathing. The contraction of the inspiratory muscles increases the volume of the lung. On the other hand elastic resistance of the lungs,

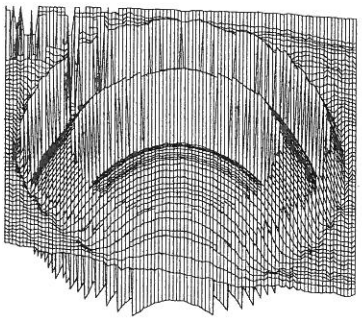

*Fig. 9.* Wrapped phase distribution

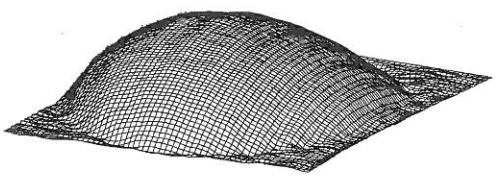

*Fig. 10.* Unwrapped phase distribution

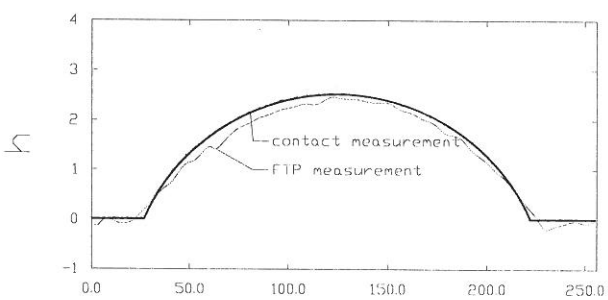


*Fig. 11.* Comparison between FTP and contact measurement

flow resistance in the airways and the sliding of tissues over one another offer resistance to the pressure developed by the inspiratory muscles. This results in negative pressure inside the pleural cavity. In patients with respiratory insufficiency is this pressure higher (more negative) as in healthy people, caused by either higher elastic forces ance in the airways.

Figure 13 indicates the relationship between lung volume and the elastic forces of the lung and of the chest wall in the human. Also shown is the resultant net balance between these two forces. In this figure, pressures tending to increase lung volume are negative, and those tending to decrease lung volume are negative. As in the model the forces exerted by the lung and

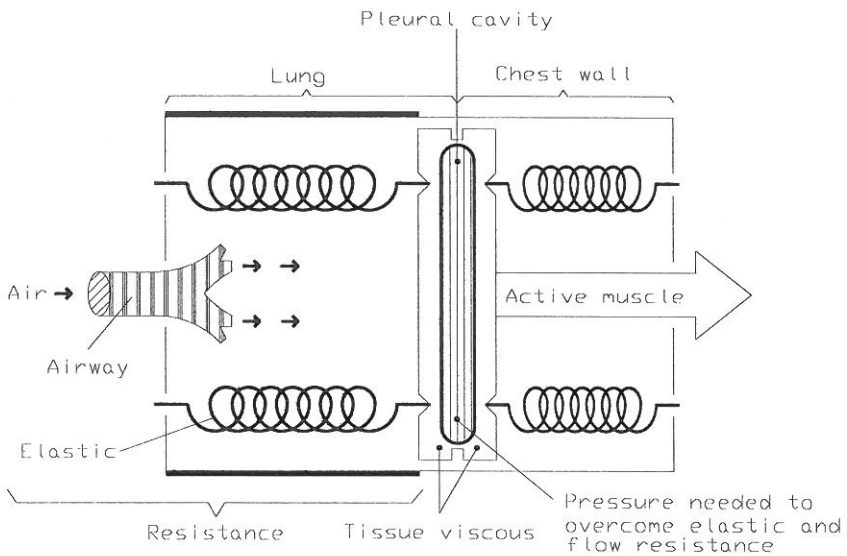


*Fig. 12.* Mechanical analogue of the resistances that must be overcome to move the air into the lungs

chest wall at the *resting level* are equal pulling in opposite directions, therefore the relaxation pressure is zero. A t lung volumes greater than the *resting level* the force of the lung tending to deflate it is greater than that of chest wall tending to inflate it, therefore the *relaxation pressure* is positive. At lung volumes less than *resting level*, outward pull of the chest wall is greater than the pull of the lungs in the expiratory direction, so that the *relaxation pressure* is negative. In addition to that, the pressures of the elastic forces of the lung in patients with respiratory inefficien y is shown. It's much greater than in healthy persons, therefore the *relaxation pressure* is much higher than normal.

Pressures in the pleural cavity represent important information in estimating level of the dis-

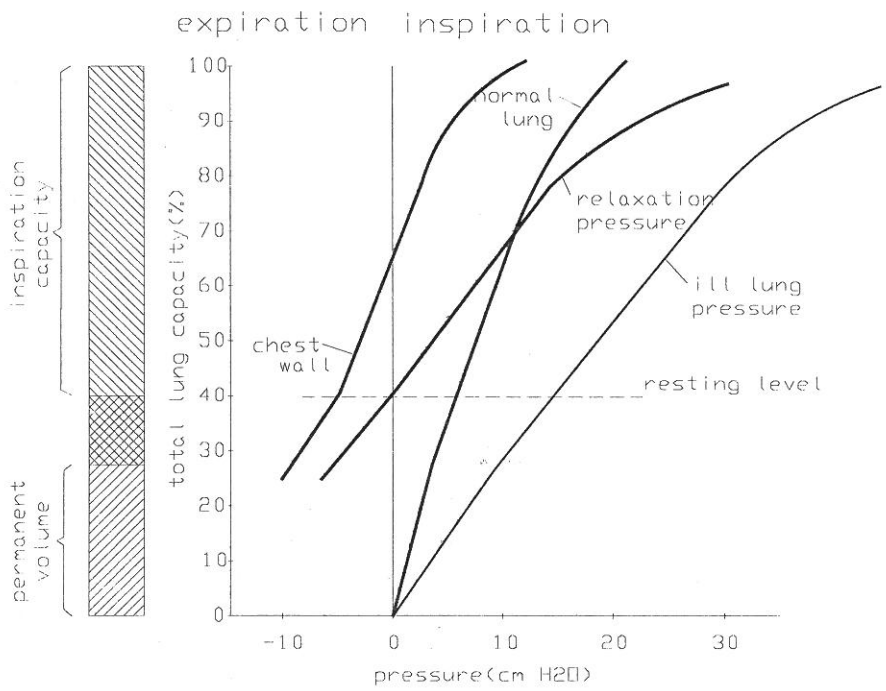


*Fig. 13.* The pressure across the chest wall and the lungs at different lung volumes

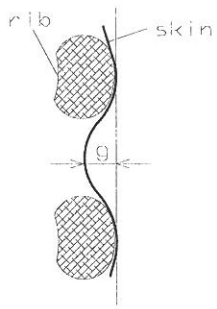


*Fig. 14.* The depression of skin between ribs

ease in patients with various respiratory inefficiencies. Unfortunately, no appropriate way of estimating this parameter exists. Common way to measure this pressure is based on inserting a straw with a baloon at the end through the nose inside the throat and measuring the pressure inside the baloon. This technique is very accurate but, needless to say, a very painful one, too. Therefore, it is often rejected by the patients. We assume that by measuring the depression between ribs we could observe the changes of pressure inside the pleural cavity.

## 4.2. Experiments

Depression of skin was measured in three position. *(1) still, (2) inspiration, (3) maximum manoeuver* — a position in which the inspiratory muscles contract but no air comes through the airways. In figure 15 deformed grating image and 3–D model of patient's depression between ribs during maximum manoeuver are presented.

## 5. Conclusions

The work compares Moiré topography and Fourier Transform Profilometry. Fourier Transform Profilometry is thoroughly described and results of experiments are presented. Furthermore, some aspects of pulmonary function testing are discussed and application of FTP within that field of medicine is shown.

The most important advantage of FTP over Moiré topography is that it is more appropriate for automated processing. Moreover, several problems associated with Moiré topography such as assigning fringe orders, locating

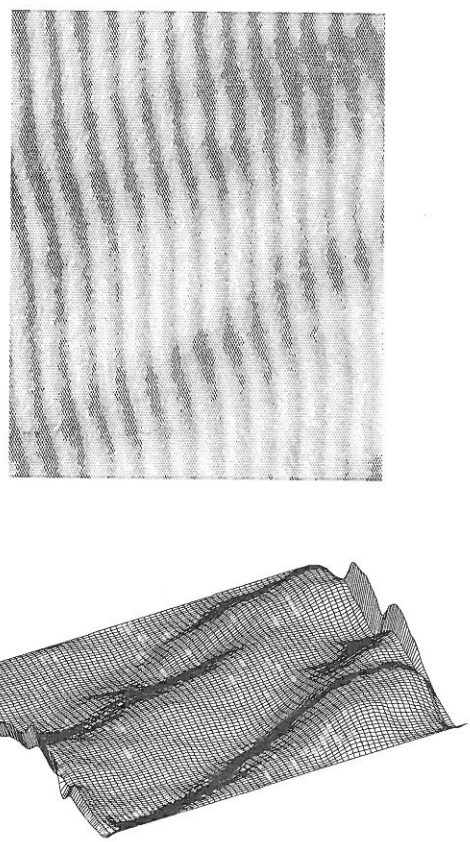

*Fig. 15.* Maximum manoeuver of a patient with respiratory insufficiency

centers of brad fringes, or interpolating regions between fringes are gone.

FTP has proved to be efficient also in measuring depression between ribs, since it has much higher sensitivity than Moiré Topography and is practically insensitive to reflection of the skin, which is very much the case in older patients.

Further work should be directed towards a definition of a model, that would show the relations between the depression of skin and pressure in the pleural cavity, which would lead us to ability to determine the level of the disease in patients with respiration insufficiencies. In definition of the model. the following parameters should be considered: type of the disease, age of the patient, and the thickness of underskin fat by each patient.

## References


[1] Meadows D.M., Johnson W.O., Allen J.B., Generation of Surface Contours by Moiré Patterns, *Applied Optics*, Vol. 9, No. 4, pp.942–947, April 1970.

[2] TAKASAKI H., Moiré Topography, *Applied Optics*, Vol. 9, No. 6, pp.1467–1472, June 1970.

[3] IDESAWA M., YATAGAI T., SOMA T., Scanning moiré method and automatic measurement of 3–D shapes, *Applied Optics*, Vol 16., No. 8, pp.2152–2162, August 1977.

[4] TAKEDA M., INA H., KOBAYASHI S., Fourier-transform method of fringe-pattern analysis for computer-based topography and interferometry, *Journal of Optical Society of America*, Vol. 72., No. 1, pp.156–160, January 1982.

[5] TAKEDA M., MUTOH K., Fourier transform profilometry for the automatic measurement of 3–D object shapes, *Applied Optics*, Vol. 22, No. 24, pp.3977–3982, December 1983.

[6] MORIMOTO Y., SEGUCHI Y., HIGASHI T., Application of Moiré analysis of strain using Fourier transform, *Optical Engineering*, Vol. 27, No. 8, pp. 650–656, August 1988.

[7] NEUGEBAUER H., WINDISCHBAUER G., *Surface Topography and Body Deformity.* Proceedings of the 5th international Symposium, Wien Sept. 29 — Oct 1, 1988. Gustav Fischer Verlag, Stuttgart, New York, 1990.

[8] SUGANUMA M., YOSHIZAWA T., Three-dimensional shape analysis by use of a projected grating image, *Optical Engineering*, Vol. 30, No. 10, pp. 1529–1533, October 1991.

[9] CHERNIACK R.M., *Pulmonary function testing*, W.B.Saunders Company, Philadelphia, 1992

[10] YOSHIZAWA T., TOMISAWA T. Shadow moiré topography by means of the phase-shift method, *Optical Engineering*, Vol. 32, No. 7, pp. 1668–1674, July 1993.



*Contact address:*

M.Leonardi, M.Fležar, A.Urbanč, J.Lenarčič
Jožef Stefan Institute
Jamova 39, Ljubljana, Slovenija
e-mail: michele.leonardi@ijs.si



MICHELE LEONARDI (1965) received his B.S. and M.Sc. from the Faculty of Electrical Engineering and Computer Science at the University of Ljubljana in '90 and '93, respectively. His research interests include image processing with applications in medicine.

MATJAŽ FLEŽAR (1963) received his M.D. 1989 from the University of Ljublja na at the Faculty of Medicine. He received his certified degree in 1990. Since 1990 he's been with the Institute for Diseases of the Chest Golnik, Sloven ia as internal medicine resident. In 1991 and 1992 he studied as a postgraduate student at University McGill, Montreal, Canada. In 1993, he spent a month in Royal Victoria Hospital v Montreal, as a visiting researcher.

ANDREJ URBANČ (1966) received his B.S. from the University of Ljubljana, Faculty of Electrical Engineering and Computer Science in '91. He is currently working as a postgraduate student researcher at the Robotics Laboratory at the Jožef Stefan Institute at the University of Ljubljana. His research interests include robot kinematics and image processing.

JADRANG LENARČIČ received B.S., M.Sc., and D.Sc. from the University of Ljubljana Engineering and Computer Science in 1979, 1981 and 1985, respectively. He has been with the Jožef Stefan Institute since 1979 and has been head of the Robotics Laboratory since 1985. He is Associated Professor at the University of Ljubljana. His main research interests include robotics in general and robot kinematics in particular. Recently, his interests include motion of human upper extremities and other investigations that relate biomechanics and robotics. He is charring a series of international symposia Advances in Robot Kinematics that is organised every other year under patronage of IFToMM. He is National Coordinator of Slovenia in the International federation of Robotics.